



HAL
open science

Slope morphologies offshore Dakhla (SW-Moroccan margin)

Massinissa Benabdellouahed, Agnes Baltzer, Marina Rabineau, Daniel Aslanian, Mohamed Sahabi, Fabien Germond, Benoit Loubrieu, Youssef Biari

► **To cite this version:**

Massinissa Benabdellouahed, Agnes Baltzer, Marina Rabineau, Daniel Aslanian, Mohamed Sahabi, et al.. Slope morphologies offshore Dakhla (SW-Moroccan margin). Bulletin de la Société Géologique de France, 2016, 187 (1), pp.27-39. 10.2113/gssgfbull.187.1.27 . hal-04200706

HAL Id: hal-04200706

<https://hal.science/hal-04200706v1>

Submitted on 5 Jan 2024

HAL is a multi-disciplinary open access archive for the deposit and dissemination of scientific research documents, whether they are published or not. The documents may come from teaching and research institutions in France or abroad, or from public or private research centers.

L'archive ouverte pluridisciplinaire **HAL**, est destinée au dépôt et à la diffusion de documents scientifiques de niveau recherche, publiés ou non, émanant des établissements d'enseignement et de recherche français ou étrangers, des laboratoires publics ou privés.

Slope morphologies offshore Dakhla (SW-Moroccan margin) Morphologies de la pente continentale au large de Dakhla (marge SW marocaine)

Benabdellouahed Massinissa^{1,2,*}, Baltzer Agnes^{1,3,*}, Rabineau Marina^{2,*}, Aslanian Daniel¹,
Sahabi Mohamed⁴, Germond Fabien¹, Loubrieu Benoit¹, Biari Youssef¹

¹ IFREMER BREST, LGG, BP70, 29280 PLOUZANE, FRANCE

² CNRS, UMR 6538, IUEM, LABORATOIRE DOMAINES OCEANIQUES, 29280 PLOUZANE, France

³ LABORATOIRE GEOLITTOMER, CNRS-UMR 6554 LETG, UNIVERSITE DE NANTES, 44312
NANTES CEDEX 3, FRANCE

⁴ LGM, DEPARTEMENT SCIENCES DE LA TERRE, FACULTE DES SCIENCES, BP 20, 24000 EL
JADIDA, MOROCCO

* Corresponding authors : Massinissa Benabdellouahed : massinissa.benhabdelhaoued@ifremer.fr ;
Agnès Baltzer : agnes.baltzer1@univ-nantes.fr ; Marina Rabineau : marina.rabineau@univ-brest.fr ;

Abstract :

This study explores a portion of the West African margin at the junction between two well-known segments offshore Dakhla and offshore Mauritania with destructional architecture characterized by giant slides. In between these two segments, the Dakhla segment has historically been described as a constructional section. During an oceanographic Dakhla cruise (2002), high resolution seismic data, swath bathymetry and imagery were acquired around latitude 23° N, offshore Dakhla. This new data set reveals the existence of varied and complex morphologies on the continental slope, interpreted as a "shallow-shaped" canyon, seafloor depressions or pockmarks, ridges and scarps. These morphologies are interpreted as clues of sedimentary transfers and rupture processes. A scenario is proposed for the development of these different sedimentary morphologies.

Keywords : African margin, Bathymetry, Seismic interpretation, Pockmarks, Ridges, Scarps

Résumé :

Cette étude s'intéresse à une portion de la marge Ouest Africaine, à la jonction entre deux segments largement étudiés situés au large de Dakhla et de la Mauritanie, caractérisés par une morphologie globale de type destructif avec de larges glissements. Entre ces deux segments, celui de Dakhla est généralement décrit comme une portion de marge de type constructif. Durant la mission océanographique Dakhla (Décembre 2002), au large de Dakhla, de nouvelles données de sismique haute résolution, de bathymétrie et d'imagerie ont été acquises autour de la latitude 23°N. Ce nouveau jeu de données révèle l'existence de différentes morphostructures du fond telles qu'un canyon, des dépressions plus ou moins circulaires (pockmarks), différents types de rides et des escarpements, structures interprétées comme autant de témoignages de processus de transferts sédimentaires et de rupture de pente.

Mots-clés : Marge africaine, Bathymétrie, Interprétation sismique, Pockmarks, Rides, Escarpements

1. Introduction

The study of slope stability along passive continental margin is important to understand 48 sediment transfer from the shelf to the oceanic basin and to approach potential geo-hazards. 49 Among them, submarine landslides affect all types of continental margins and landslides are 50 relatively larger on passive margins than along active margins [Masson *et al.*, 2009]

52 Compared to all passive margins, the North-western African continental margin is
53 characterized by large submarine landslides ($>400 - 600 \text{ km}^3$) such as the Sahara Slide, the
54 Cape Blanc Slide, the Mauritania Slide, and the Complex Dakar Slide, which are intensively
55 studied since the 1970's [e.g. Antobreh and Krastel, 2006; Embley, 1982; Gee *et al.*, 2001;
56 1999; Georgiopoulou *et al.*, 2010; 2009; Hühnerbach *et al.*, 2004; 2004; Jacobi and Hayes,
57 1992; Krastel *et al.*, 2012; Wynn *et al.*, 2000]

58 In the northern part of the west African coast, south of the Canary Islands and offshore
59 Dakhla, around 25°N , the margin shows a destructional margin architecture [Ranke *et al.*,
60 1982] with a steep irregular profile and numerous slumps and slides cutting the slope surface
61 such as the Sahara slide [Georgiopoulou *et al.*, 2010; Wynn *et al.*, 2000]. In the southern
62 zone, south of 21°N and offshore Mauritania, two slides have been described by Krastel *et al.*,
63 [2006] and Antobreh and Krastel [2006], the Cap Blanc slide and the Mauritania slide.

64 Between these two zones, where instabilities are related to relatively high accumulation rates
65 but rare triggers, [Ranke *et al.*, 1982] described a constructional section of the margin with
66 smooth convex/concave shape and evidences of shelf and slope progradation.

67 During the Dakhla cruise [2002] devoted to deep investigation of the margin on the R/V
68 Suroit, high resolution seismic data together with swath bathymetry were additionally
69 acquired on a relatively unknown portion of the margin, at 23°N offshore Cap Blanc and
70 Dakhla (Fig. 1). This new data set reveals new morphologies linked to different types of
71 sedimentary transfer processes, that are described in this paper. A scenario is proposed to link
72 these different morphologies, with relative ages.

73

74 **GENERAL SETTINGS**

75 The West African margin is one of the oldest passive margins in the world: the rifting phase
76 of this margin occurred between the late Triassic and the Early Jurassic and was followed by

77 oceanic spreading initiated around 195 Ma [Labails, 2007; Labails *et al.*, 2010; Sahabi *et al.*,
78 2004]. Earthquakes are rare and have been recorded in the old weakness zones created during
79 the opening of the Atlantic Ocean [Hayes and Rabinowitz, 1975]. From Jurassic to Early
80 Cretaceous, carbonate platforms have been constructed, followed by marine clastic infill
81 between Cretaceous and Tertiary. Since the late Cretaceous, erosive cycles have shaped the
82 margin [Labails, 2007; Labails *et al.*, 2010] and a major eocene erosional surface [Labails,
83 2007], observed on the opposite American margin by Mountain and Tucholke, [1985], is
84 associated to a succession of gullies and canyons perpendicular to the margin.

85 On the Dakhla coast (Fig. 1), the shelf-break is located at 100-200 m of water depth. Beyond,
86 the continental slope has a width of 50-250 km [Wynn *et al.*, 2000], and displays slope angles
87 of 1-6°. In some areas, e.g. adjacent to the Sahara Canyon System, slope angles may reach
88 14°. The slope evolves to the continental rise at water depths of 1500-4000 m, with gradients
89 decreasing from about 1° on the lower slope/upper rise, to 0.1° on the lower rise [Masson *et*
90 *al.*, 1997]. The rise is generally 100- 1500 km wide and terminates at water depth of 4500-
91 5400 m, the deep abyssal plains.

92 Offshore the Dakhla margin, quaternary deposits are constituted of pelagic and hemipelagic
93 sediments [Georgiopoulou *et al.*, 2010; Wynn *et al.*, 2000]. This fine-grained clastic slope
94 apron, with pelagic/hemipelagic ‘background’ sedimentation is overprinted by downslope
95 gravity flows, shaped by along slope bottom currents [Wynn *et al.*, 2000]. Zühlsdorff *et al.*,
96 [2008] showing successions of turbiditic and hemipelagic deposits in the Cap Timiris Canyon
97 system that were correlated to the alternation of arid and humid climatic conditions. They
98 explained that both atmospheric systems: the northerly Trade winds and the southerly African
99 monsoon, interact with each other and with seasonal shifts: northwards during times of boreal
100 summer (or climatically forced on larger time scales) due to Trade winds weakening and
101 southwards when the Trade winds strengthen. The effect for western Africa is humidification

102 when monsoonal pattern prevails and aridification when Trade winds become stronger
103 [Zühlsdorff *et al.*, 2008].

104 Offshore Mauritania, high accumulation areas of biogenic detritus have also been observed at
105 water depths of 1000-1500m in relation with intense upwelling activity in the area [Fischer *et*
106 *al.*, 2009; Henrich *et al.*, 2008]. Oceanic upwelling is seasonally and spatially variable on the
107 northwest margin [Mittelstaedt, 1991; Van Camp *et al.*, 1991] with a major upwelling zone as
108 seen on figure 1. The region off Cap Blanc is dominated by a persistent upwelling and strong
109 activity of small-scale eddies, filament and jets [Karakas *et al.*, 2006]. The area between 26°N
110 and 21°N shows that a permanent upwelling has been recorded since 2002 and reported by the
111 Bulletin of Upwelling, [2015]. High sediment accumulations areas of biogenic detritus are
112 also observed at 1000-1500 m water depths (mwd) in relation with intense upwelling activity
113 in the area [Fischer *et al.*, 2009].

114 Thus, the large open-slope landslides (>400-600 km³) occurring on this continental slope
115 (Fig. 1), like the Mauritania, Cap Blanc and Sahara Slides [Embley, 1982; Gee *et al.*, 1999;
116 Georgiopoulou *et al.*, 2009; Georgiopoulou *et al.*, 2007; Henrich *et al.*, 2008; Krastel *et al.*,
117 2006] largely consist in remobilized hemipelagic sediments [Gee *et al.*, 1999; Krastel *et al.*,
118 2006].

119 The Canary Islands contribute to the sedimentation by an input of volcanoclastic material by
120 both large-scale landsliding [Wynn *et al.*, 2002] and slow fallout through the water column
121 into the hemipelagic sediments.

122 Together with the presence of these islands and seamounts, the existence of deep-water
123 bottom currents locally influence the sedimentation pattern of this margin.

124 The general water mass structure of the northwest African margin includes at about 600-700
125 mwd the southward-flowing North Atlantic Central Water (NACW), at 2000-3800 mwd, the
126 North Atlantic Deep Water (NADW) flowing in a southerly direction, and below 3800m, the

127 Antarctic Bottom Water (AABW) flowing in a northeasterly direction. These bottom currents
128 have velocities ranging from 1 to 6 cm/s [Lonsdale, 1982; Sarnthein *et al.*, 1982].
129 Oceanic upwelling is seasonally and spatially variable on the northwest margin [Mittelstaedt,
130 1991; Van Camp *et al.*, 1991] (blue dashed line on Fig. 1). A major and persistent upwelling
131 center in the region off Cap Blanc is characterized by strong activity of small-scale eddies,
132 filament and jets [Karakas *et al.*, 2006] and between 26°N and 21°N a permanent upwelling
133 has been recorded since 2002 and reported by the Bulletin of Upwelling [2015].

134

135 **DATA AND METHODS**

136 ***EM300***

137 The EM300 is a multi beam swath sonar mapping system which gives a high-resolution
138 bathymetry and an acoustic backscatter imagery. This system uses a single 30 kHz Mills
139 Cross array and is able of swath mapping at depth ranges between 10 and 5000 m. When
140 operated down to approximately 5000 m depth swath widths are about 5000 m. It runs with
141 up to +/- 75° angular swath with 135 beams per ping, and features dynamically variable beam
142 with configuration range from 1° to 4°, to achieve both high spatial resolution in deep and
143 shallow waters. The Bathymetry of Dakhla Cruise is processed with Caraïbes software
144 (developed by Ifremer) and have a spatial resolution better than 50 m (in water depths
145 <2000 m).

146 **Chirp**

147 The Chirp is a hull-mounted sediment echosounder. The signal is characterized by a long
148 impulse (50 ms), lineari modulated in time and frequencies. Thus, its frequency spectrum
149 ranges 2-5.2 kHz with an average at 3.2 kHz. This frequency bandwidth allows a very high
150 resolution (dm) in surficial layers (high frequency) and a deep penetration with the lower
151 frequency that may reach about 100 m. 39 profiles (Fig. 1) have been recorded equivalent to

152 229 hours of data. For display purposes the envelope of the signal is computed and low-pass
153 frequency filtered (2000 Hz). No automatic gain control is applied to the data, to avoid
154 blanking features close to the seafloor reflection.

155

156 **Multichannel seismic data**

157 A total of 1500 km of multichannel seismic profiles (**Fig. 1**) were shot during the Dakhla
158 cruise on board the N/O Suroit in 2002 [Klingelhoefer *et al.*, 2009; Labails 2007; Labails *et*
159 *al.*, 2010]. The system was composed of a 4.5 km long streamer of 360 channels, with a 12.5
160 m group interval, which was towed at 15 m immersion. The data were sampled at 4 ms.

161 Two different marine seismic sources were used during the cruise. For the deep crustal targets
162 a large (8100 in³) airgun array was used in the single bubble mode consisting of 12 airguns
163 between 250 in³ and 976 in³ (16 l). The airgun array was shot at a constant interval of 150 m.

164 Processing of the multichannel seismic data was performed using the Sispeed package. It
165 included spherical divergence correction, FK-filtering, band-pass filtering (3-5-50-60 Hz),
166 internal mute and dynamic corrections. The last processing steps included applying an
167 automatic gain control and a Kirchoff migration using water or stacking velocities.

168

169 **RESULTS**

170 **Morpho-sedimentary structures**

171 The study area is characterized by a broad continental shelf, with a width ranging from 50 to
172 80 km and a shelf break at a water depth of 100-120 m. The swath bathymetry map of the
173 continental slope, with a 100 m grid cell size resolution, reveals a complex seafloor
174 morphology from the shelf break at 120 m to 3000 m (**Fig. 2**).

175 The bathymetric map (Fig. 2) shows an undulating morphology that can be described as a
176 bulge-like structure with a large radius of curvature of around 40 km shown on the profile (ef)
177 (Fig. 2). This undulating morphology is oriented NW-SE, perpendicular to the shoreline.
178 Based on the slope map and the bathymetric profiles, we divide this portion of the continental
179 slope in three sections (Fig. 2 – profile (ab):
180 - the first section, between 120 and 500 m water depth, is characterized by a slope angle of 5°
181 and corresponds to the lower slope.
182 - the second section, between 500 and 2100 mwd, is characterized by a slope angle ranging
183 from 2° to 4° , with a convex longitudinal shape from 1000 to 2000 (profiles ab and cd,
184 Fig. 2) and a complex bulged shape seen on transversal profiles (ef) and (gh) (Fig. 2).
185 - the third section, between 2200 and 3000 mwd, is characterized by a gentle slope, less than
186 2°, with well-marked scarps (S1 and S2, Fig. 2). The southern part of the study area, between
187 2600 and 3000 mwd, is characterized by the presence of a meandering channel.
188 From upslope to downslope, four sea floor features are identified, on the morphobathymetric
189 map (Fig. 3), 1) the "shallot-shaped" canyon, 2) the sea floor depressions, 3) different ridges
190 types and 4) scarps which will be described in the following paragraphs.

191

192 **Scarps**

193 The morphobathymetric map shows the presence of two scarps (i.e. S1 and S2, Fig. 3) that cut
194 the downslope part respectively between 2400 and 2600 mwd and between 2100 and 2600
195 mwd (Fig. 3). They both show a general N-S trend, with a complex broken shape almost
196 imbricated.

197

198

199

200 **Dakhla "shallow-shaped" canyon:**

201 This canyon deeply incises the northern portion of the studied area, between 800 and
202 2200 mwd (Fig. 4). This canyon, named the "shallow-shaped" canyon because of its specific
203 shape, is globally oriented E-W and can be spitted in three sub-parts: a proximal part, a
204 median part and a distal part.

205 The proximal part of the canyon runs from 800 m down to 1000 m axial depth (Fig. 4) and
206 displays a V-shaped with a steep flank to the South (4° ; 100 m-deep axial incision) and a
207 terrace to the North (Fig. 4 profile ab).

208 The median part, from 1000 m to 1400 mwd (Fig. 4), corresponds to the enlargement of the
209 incising feature reaching up to ten kilometers with smoother slope (axial incision $<2^\circ$) and
210 edges. Profiles (cd) and (ef) show a 40 m-deep axial incision.

211 On the distal part, from 1400 to 2200 mwd (Fig. 4), the incision narrows down to a single
212 channel seen on profile (gh).

213

214 **Ridges morphologies:**

215 Two groups of ridges may be observed on the figure 5.

216 The first one, from 1000 to 1300 m, is only visible on the bathymetric map (nor on the chirp
217 profiles because of the rough weather and neither on the slope map), in the eastern part of the
218 central bulge (5A). These small scale ridges reveal a regular morphology of 3 to 5 m high for
219 a wavelength of 50 m, with a N30 orientation, thus oblique to the main slope (Fig. 5A).

220 A second group of ridges, larger and irregular, occur between 1500 and 1800 mwd. These
221 ridges are larger, with 1-12m high with kilometeric lengths (2-20 km) and spaced by 1 to 5 km.
222 They show a perpendicular orientation to the main slope (Fig. 5A, western part).

223

224

225 **Seafloor depressions:**

226 Asymmetric seafloor depressions have been observed in the central part of the area around
227 1500 mwd (Fig. 5B). Three types of seafloor depressions have been mapped and detailed on
228 figure 5B: 1) circular (Fig. 5 – profiles 3 and 4) with a diameter varying from 0.5 to 1 km, 2)
229 troughs 0.5–1.5 km wide, 6–9 km long and up to 45 m deep; oblique to the slope, oriented
230 SW/NE and 3) troughs parallel to the slope.

231

232 **Echo Types classification**

233 The studied area can be divided into several zones based on the dominant echo types. Five
234 echo types (Fig. 6 - for location see Fig. 3) have been identified and grouped within the four
235 main classes following the classification of Damuth [1980] and Damuth and Hayes [1977]:
236 distinct (I), hyperbolic (II), transparent (III), indistinct (IV). Each acoustic facies is described
237 using amplitude, lateral continuity, frequency and geometry of the sub-bottom echoes (Fig. 6).

238

239 *Distinct echoes (I)*

240 Those echo types are characterized by a distinct sharp continuous bottom echo with parallel
241 sub-bottom reflectors. It has been further subdivided into two sub-types (Fig. 6).

242 Facies I-1 is a laminated facies constituted by alternation of parallel continuous thin high and
243 low amplitude reflections up to 60 ms thick.

244 This facies covers a large part of the study area, from the base of the continental slope to the
245 western most part of the area. The reflections have slightly higher amplitude than in deeper
246 water depths, between 800 to 2200 and 2200 to 3000 mwd. This facies covers the wavy
247 morphologies (ridges area), seafloor depressions and scarps.

248 Facies I-2 is similar to facies I-1 with alternation of parallel continuous thin high- and low
249 amplitude reflectors, but is topped by a transparent upper layer (0.0025 ms), with a thick and
250 diffuse seafloor reflector. This facies is mapped between 1600 and 2200 mwd.

251 *Hyperbolic echoes (II)*

252 This echo is characterized by irregular overlapping hyperbolae with chaotic sub-bottom
253 reflections of relatively high amplitude. The signal shows slight even none sea-floor
254 penetration (Fig. 6). It is restricted to the area of the shallot-shaped canyon.

255 *Hard echoes (III)*

256 It has been subdivided into two sub-types (Fig. 6)

257 Facies III-1 is characterized by high-amplitude reflectors with no sub-bottom echoes and/or
258 diffuses returns on seismic profiles and a rough seafloor. It occurs on the upper continental
259 slope and shelf break.

260 Facies III-2 displays hard echoes with subbottom reflectors, this echo type shows
261 discontinuous and inclined subsurface reflectors, appearing as discontinuous patches. Facies
262 III-2 is mainly represented on the continental shelf of our study area.

263

264 **INTERPRETATION**

265 **Sedimentary structures**

266 High-resolution multibeam and bathymetry data show a highly-complex superficial
267 morphology described above. In order to understand the origin of those sedimentary
268 structures, we use deep penetrating multichannel seismic profiles (Figs. 7 and 8). The seismic
269 profile AB (Fig. 7) can be divided in two parts: the lower part, below the cretaceous reflector
270 [Labails, 2007], displays long amplitude undulations that are related to the presence of a
271 tectonic bulge described by several authors [e.g. Jolivet *et al.*, 1984; Patriat and Labails,
272 2006]. On the other hand, the upper part of the profile AB (Fig. 7) shows undulations of the

273 sedimentary layers with wavelengths of about 40 km, probably related to a geological heritage
274 with the presence of numerous canyons and interfluves (Fig. 7). This large-scale undulating
275 morphology is locally complemented by peculiar features described in previous paragraphs:
276 two scarps, the "shallot-shaped" canyon, the ridges and the seafloor depressions. The aim of
277 the discussion will be to try to understand each of the sedimentary process triggering these
278 deposit features.

279

280 **The scarps morphologies**

281 The two scarps (S1 and S2) correspond to 30- 40 m steps which are observed on the seismic
282 profile CD (Fig. 8). The seabed and shallow reflectors are separated by shallow faults or
283 hydro-fracturing due to fluid pressure that connect to surface discontinuities (sliding surfaces;
284 Figs. 7 and 8). The scarps morphologies have affected the continuous echoes i.e. seismic
285 facies I-1 and I-2 (Fig. 8). According to the literature, Facies I-1 and I-2 generally correspond
286 either to an alternations of pelagic/hemipelagic (muddy/silty) sediments or to turbidites
287 deposits [e.g. Damuth, 1980]. The reflectors (pelagic/hemipelagic facies) that drape S1 are cut
288 by S2 can be observed on the seismic profile (Fig. 9). This observation proves that Scarp S1 is
289 older than S2.

290

291 **Shallot-shaped canyon**

292 The "shallot shaped" canyon (Fig. 4) corresponds in its proximal part, to a group of V- shaped
293 incisions similar to the gullies described on other continental slope by [Twichell and Roberts,
294 1982]. They are issued from the shelf edge and further join together into a single canyon
295 going downslope and finally reach the abyssal plain in its distal part. The sharp incision of the
296 canyon (ab) does not show any sedimentary pelagic drape on the chirp profiles, The median
297 part of the shallot-shaped canyon is characterized by an hyperbolic echo (type II, Fig. 6)

298 interpreted by several authors [Damuth, 1980; Jacobi, 1976] as a rough seafloor covered with
299 coarse elements such as blocks or mass-transport deposits so-called debrites [Lee *et al.* 1999].
300 The chaotic nature of the echo in the shallot-shaped canyon suggests a high degree of
301 sediment remobilization and thus deposition from turbidity currents or debris flows. Collapse
302 of the canyon flanks (see Fig. 3 for location) may contribute to the widening of the channel
303 and to the irregular deposit morphology. Following Lonergan *et al.*, [2013], we propose that
304 the gullies channelize turbidity currents originating from the shelf, supplying sediments
305 downslope in relation with intermittent activity. The coarser elements are deposited in the
306 median part (Fig. 4), while the rest flowing down evolves into turbidity currents by
307 incorporating water and transforming its matrix into a fluid, which goes through the canyon
308 (profile gh – Fig. 4), in the distal part of the system like the scenario described by Mulder and
309 Alexander [2001].

310 No clear scar, headwall or departure zone has been identified on bathymetric data to explain
311 mass wasting processes on the upper slope, therefore the simplest way to explain the presence
312 of debris flow deposits would be the connection with a continental supply system with
313 sporadic but intense and extreme events.

314 Turbidity current pathways were inferred in this area but not connected to permanent present
315 day drainage system on land because of the saharian desertic climate [Wynn *et al.*, 2000].
316 Thus, the origin of many submarine canyons, on this continental margin of north-west Africa
317 between 15°N and 26°N, like Cap Timiris Canyon, are assumed to be related to a major sub
318 aerial river system that was active in the past in relation with "green sahara" periods since
319 Plio-Pleistocene times [Antobreh and Krastel, 2006; Larrasoaña *et al.* 2013; Vörösmarty *et*
320 *al.*, 2000]. Recent studies [McGee *et al.*, 2013; Skonieczny *et al.*, 2013] revealed that eolian
321 dust fluxes varied a lot during the last 20 ka, with maximum values during Heinrich Stadial 1

322 and the Younger Dryas, and minimum fluxes during the end of the African Humid Period
323 between 8 and 6 ka.

324

325 **The seafloor depressions**

326 Sea-floor depressions observed around the 1500 m isobath reveal two types of shape (Fig. 5).

327 The circular shaped depressions may be assimilated to pockmarks features. Pockmarks are

328 circular to elongated seafloor depressions which are often associated with fluid gas escape

329 flow from the subsurface [Judd and Hovland, 2007]. The bright amplitudes seen on the figure

330 9 may correspond to hard lithology like seep carbonates which would likely be associated

331 with gas venting [Cathles *et al.*, 2010; Çifçi *et al.*, 2003; Çifçi *et al.*, 2003; Gay *et al.*, 2006;

332 Hovland *et al.*, 2010; Hovland *et al.*, 2002; Judd and Hovland, 2007]. An unconformity is

333 observable on the seismic chirp profile (Fig.9) around 1.95 twt (s) (1500 mwd).

334 To explain the formation of the second type of depressions, the elongated ones (Fig. 5), we

335 examine three hypotheses. The concentration of circular pockmarks can cause the formation

336 of the elongated pockmarks observed at 1500 m. The Fig. 5B shows an outstanding example

337 of the evolution of pockmarks from circular to elongated shape. The addition of two

338 pockmarks may be observed before complete coalescence on the profile 2 (Fig. 5C) and a

339 detailed observation show that the large pockmark (Fig. 5B) is composed of a coalescence of

340 ten to twenty smaller depressions. This first hypothesis corresponds to groups or long chains

341 of pockmarks described by [Hovland and Judd, 1988].

342 Another hypothesis is that these linear depressions reflect the surface expression of a deeper

343 structure such as a meandering channel or a subjacent fault draped by sediment, as suggested

344 by the third cartoon on the top of the figure 8. Meandering paleo-channels are clearly seen on

345 the figures 3 and 5A and may explain the occurrence of some of the elongated seafloor

346 depressions.

347 The dissymmetry or "*en échelon*" or "*festooned*" appearance of this succession of holes and
348 troughs depressions have already been observed on a portion of this margin, between Cap
349 Timiris and Nouakchott by Yang and Davies [2013]. They described troughs, either parallel
350 or oblique to the slope dip, with elongate *en-echelon* plan-forms. These troughs have variable
351 length, ranging from 0.5 to 10 km and are related to 2 types of gravity-driven faults: tear
352 faults and normal faults. Based on 3D seismic data, these authors analysed a set of times
353 slices with amplitude maps and suggest that the "*en echelon* and linear" troughs were formed
354 as a result of multiple episode of down slope creep and have propagated through 60-140 m of
355 sediments. These observations area in close agreement with our data, suggesting that the
356 seafloor depressions may be assimilated to a potential rupture line and represent the surface
357 expression of tear and/or linear faults affecting the upper sedimentary column. The location of
358 "*en echelon* and linear" troughs at the slope inflexion (around 1500m) may suggest the
359 departure zone of a sliding event.

360

361 **Ridges areas :**

362 The two ridges areas are observed on both sides of the sea-floor depressions area (Figs. 5).
363 Upper slope ridges, smaller in size and presenting an oblique orientation to the slope are
364 assimilated to sediment-wave morphology, which would be in agreement with the existence
365 of numerous sediment-wave fields mapped in the northern part of the margin by [Wynn *et al.*,
366 2000]. These morphologies are commonly reported on the continental slopes of passive
367 margins [Faugères *et al.*, 2002; Faugères *et al.*, 200; Viana and Rebesco, 2007] and active
368 margins [Lee and Chough, 2001]. The bad weather prevent any further investigation of these
369 small ridges features on the chirp data and thus, our observations are only based on the
370 bathymetry map.

371 The second group of ridges, larger in size are located from 1500 to 1800 mwd. These
372 undulations are parallel to the bathymetry and occur just below the seafloor depressions area
373 (Fig. 5), traducing a deformation of the superficial sedimentary cover. We suggest they may
374 be interpreted as compressional ridges.

375

376 **DISCUSSION**

377 All those sea-floor features, pockmarks, compressive ridges and scarps, canyons, reveal the
378 existence of sediment transfer and instability processes from upslope to downslope. Here we
379 suggest a potential link between these specific morphologies.

380 According to the literature, non-random pockmarks show spatial arrangement related either to
381 complex underlying geology or to local disturbance of the seabed, whereas random
382 distribution of pockmarks is commonly displayed on the lower slope where sediments are
383 generally fine-grained and tectonic structures are rare [Pilcher and Argent, 2007].

384 In our study area, pockmarks are arranged along a "festooned line" on a N-S direction
385 parallel to the bathymetry. However the seismic SMT profiles (Figs. 7 and 8) do not show
386 deep faults or tectonic structures with complex underlying geology. The only visible fault is
387 the one displayed in the scarp S2 (Fig. 8 - cartoon 2) and it appears to shift the first three
388 reflectors). This fault is therefore considered as superficial and might be rooted in a layer
389 which constitutes a sliding surface (basal detachment) seen on the figure 8.

390 Pilcher and Argent [2007] described linear pockmark trains which are associated with listric
391 slump faults in different cases of continental slope instability. We suggest that scarps S1 and
392 S2 are former zones of pockmarks alignments (Fig. 10).

393 The "festooned line" or "en-échelon" line of coalescent pockmarks could witness a weakness
394 zone on the slope which could evolve into a future detachment area and form a new scarp S3.

395 This phenomenon of high concentration of pockmarks (causing their fusion) is widely
396 observed e.g. in the Congo Basin [Gay *et al.*, 2006; Gay *et al.*, 2003], Nigeria margin [Sultan
397 *et al.*, 2014; Wei *et al.*, 2015] in the Northwestern Atlantic [Fader, 1991], the Ionian Sea,
398 Greece [Hasiotis *et al.*, 2002], the North Sea [Hovland, 1984; Hovland *et al.*, 1987; Hovland
399 and Sommerville, 1985] and the Mediterranean [Dimitrov and Woodside, 2003].

400 The occurrence of compressive ridges below the pockmarks area also evidence initiation of
401 gravitary movement.

402 The main triggering mechanism for slope instability and thus gravity mass movements
403 processes, across the NW-African continental margin, is believed to be the overload of
404 sediment [Georgiopoulou *et al.*, 2010; Masson *et al.*, 2010]. Whereas, other triggers such as
405 earthquakes, free gas, gas hydrates or diapirism are believed to be of minor importance
406 [Georgiopoulou *et al.*, 2010; Krastel *et al.*, 2006].

407 During the late Pleistocene, the repeated slope instabilities appear as a common characteristic
408 of NW African margin [Antobreh and Krastel, 2006; Georgiopoulou *et al.*, 2010; 2007]. This
409 margin has also been strongly affected by Quaternary sea-level cycles [Church and White,
410 2006; Wien *et al.*, 2006]. According to Georgiopoulou *et al.* [2010], sea level changes appear
411 to be important and giant slides appear to coincide with periods of deglaciation. During the
412 latter periods, the sedimentation occurred in the vicinity of the present shore line
413 [Georgiopoulou *et al.*, 2010]. Thus, major sedimentary events on the northwest African
414 margin appear coincident with glacial - to - interglacial transitions [Church and White, 2006;
415 Georgiopoulou *et al.*, 2010]. According to Riboulot *et al.* [2014; 2013; 2012], the upper-
416 Pleistocene 100 ka cyclicity sea-level changes are the predominant driving factor of pockmark
417 formation in the Gulf of Lions and Nigeria. On the basis of these observations, we suggest
418 that Pleistocene sea level and sediment load associated with fluids escapes are the main
419 process for soft-sediment deformation off Dakhla.

420 No core or drilling wells are available in the study area, however we propose correlations
421 based on sea-level curves. The main goal of this correlation is to propose an age for the scarps
422 morphologies and pockmarks formation (Fig. 10).

423 Riboulot *et al.*, [2013] have estimated the formation of a pockmark to last ~100 ka. Based on
424 that assumption, we correlate morphologies with the sea-level curve from Waelbroeck *et al.*
425 [2002] and propose the following chronology (Fig. 10):

426 - A) During the Marine Isotopic Stage MIS8 to MIS7: formation of the first generation of
427 pockmarks caused by sedimentary load at 2600 mwd, that induced the formation of a sliding
428 plane of the scarp 1. This scarp is draped by hemipelagic deposits;

429 - B) During the MIS 6 to MIS 5: formation of the second generation of pockmarks at 2200
430 mwd, that induced the formation of a sliding plane of the scarp 2. And folding of the
431 hemipelagic layer.

432 - C) During the MIS 4-2 to MIS 1 : formation and the alignment pockmarks at 1500 mwd and
433 future scarp S3 (?). This area of pockmarks is contemporary to Sahara Slide, El Golfo /
434 Canary Debris Flow and the Mauritania Slide [Siddall *et al.*, 2003].

435 During low sea level phases, cannibalization of the shelf combined with "green sahara"
436 periods since Plio-Pleistocene times (Larrasoña *et al.* 2013) induced an overload of sediment
437 on the slope that may have favored sediment failures. The slope destabilization might also be
438 linked to the liberation of hydrate dissociation by variation of temperature and pressure,
439 linked to glacial/interglacial phases.

440

441

442

443

444

445 **CONCLUSION**

446 The analysis of multibeam bathymetry, high-resolution sub-bottom and seismic data on the
447 continental slope of the off Dakhla allowed us to identify several morphologies such as
448 shallot-shaped canyon, pockmarks, wavy morphologies and two scarps (S1 and S2). A
449 detailed observation of these morphologies on chirp sub-bottom profiles and seismic data
450 shows evidences rupture processes and transfer of sediments. Compressive ridges is primary
451 linked to deformation mechanisms and creeping movements. This deformation is probably
452 enhanced by the presence of fluids or gas associated with internal discontinuities acting as
453 basal shear planes for creeping events. The scarps S1 and S2 indicate at least two generations
454 of slides on this margin. We suggest that slide development was caused by rapid sea level rise
455 after glaciation periods when sedimentation rate was maximum on the slope. This
456 sedimentary load induced fluid or gas migrations along unconformities and superficial faults
457 in the sediment. Fluid migration has lead to the formation and concentration of aligned
458 pockmarks in weakness zones. These slides are believed to be 100-ka cycle events controlled
459 by sea level variations during the second half of the quaternary period.

460 However, more regional studies using high resolution but deeper seismic penetration are
461 needed in the area as well as coring and geotechnical studies to fully assess the timing of the
462 events, the existence of gas hydrates and to determine whether creeping is still active today.

463

464 **Acknowledgement**

465 Special thanks are due to the captains of the N/O Suroit and Nadir and their crews together
466 with the Genavir technical staff during the Dakhla cruise. This work was partly funded by
467 Total in the frame work of the IFREMER/TOTAL Dakhla project. Authors would like to
468 thank Bruno Marsset for his help on seismic processing and Frauke Klingelhofer, Jean Nizou
469 for their comments on an earlier version of the manuscript. The two reviewers A. Gay and P.

470 Imbert and the editor O. Lacombe are thanks for their fruitful comments that helped us to
471 improve this paper.

472

473

474

475 **REFERENCES**

- 476 ANTOBREH, A.A. & KRASTEL, S. (2006). - Morphology, seismic characteristics and
477 development of Cap Timiris Canyon, offshore Mauritania: A newly discovered canyon
478 preserved-off a major arid climatic region. *Marine and Petroleum Geology*, **23**, 37–59, doi:
479 10.1016/j.marpetgeo.2005.06.003.
480
- 481 BALTZER, A., TESSIER, B., NOUZÉ, H., BATES, R., MOORE, C. & MENIER, D. (2005). -
482 Seistec seismic profiles: a tool to differentiate gas signatures. *Marine Geophysical*
483 *Researches*, **26**, 235–245.
484
- 485 BULLETIN OF UPWELLING. (2015). - Bulletin halieutique. INRH, février 2015, Maroc.
486 CATHLES, L.M., SU, Z. & CHEN, D. (2010). - The physics of gas chimney and pockmark
487 formation, with implications for assessment of seafloor hazards and gas sequestration. *Marine*
488 *and Petroleum Geology*, **27**, 82–91.
489
- 490 CHURCH, J.A. & WHITE, N.J. (2006). - A 20th century acceleration in global sea-level
491 rise. *Geophysical research letters*, **33**.
492
- 493 ÇIĞCI, G., DONDURUR, D. & ERGÜN, M. (2003). - Deep and shallow structures of large
494 pockmarks in the Turkish shelf, Eastern Black Sea. *Geo-Marine Letters*, **23**, 311–322.
495
- 496 DAMUTH, J.E. (1980). - Use of high-frequency (3.5–12 kHz) echograms in the study of
497 near-bottom sedimentation processes in the deep-sea: a review. *Marine Geology*, **38**, 51–75.
498
- 499 DAMUTH, J.E. & HAYES, D.E. (1977). - Echo character of the east Brazilian continental
500 margin and its relationship to sedimentary processes. *Marine Geology*, **24**, 73–95.
501
- 502 DIMITROV, L. & WOODSIDE, J. (2003). - Deep sea pockmark environments in the
503 eastern Mediterranean. *Marine Geology*, **195**, 263–276.
504
- 505 EMBLEY, R.W. (1982). - Anatomy of some Atlantic margin sediment slides and some
506 comments on ages and mechanisms. *In: Marine Slides and Other Mass Movements*. Springer,
507 189–213.
508
- 509 FADER, G.B. (1991). - Gas-related sedimentary features from the eastern Canadian
510 continental shelf. *Continental Shelf Research*, **11**, 1123–1153.
511
- 512 FAUGÈRES, J.-C., GONTHIER, E., MULDER, T., KENYON, N., CIRAC, P., GRIBOULARD, R.,
513 BERNE, S. & LESUAVE, R. (2002). - Multi-process generated sediment waves on the Landes
514 Plateau (Bay of Biscay, North Atlantic). *Marine Geology*, **182**, 279–302.
515
- 516 FISCHER, G., REUTER, C., KARAKAS, G., NOWALD, N. & WEFER, G. (2009). - Offshore
517 advection of particles within the Cape Blanc filament, Mauritania: Results from observational
518 and modelling studies. *Progress in Oceanography*, **83**, 322–330, doi:
519 10.1016/j.pocean.2009.07.023.
520
- 521 FURSTER, A., ELLIS, R., HENRICH, R., KRASTEL, S. & KOPF, A. (2010). - Geotechnical
522 characterization and strain analyses of sediment in the Mauritania Slide Complex, NW-
523 Africa. *Marine and Petroleum Geology*, **27**, 1175–1189.
524

525 GAY, A., LOPEZ, M., COCHONAT, P., SULTAN, N., CAUQUIL, E. & BRIGAUD, F. (2003). -
526 Sinuous pockmark belt as indicator of a shallow buried turbiditic channel on the lower slope
527 of the Congo Basin, West African Margin. *Geological Society, London, Special Publications*,
528 **216**, 173–189.

529
530 GAY, A., LOPEZ, M., ONDREAS, H., CHARLOU, J.-L., SERMONDADAZ, G. & COCHONAT,
531 P. (2006). - Seafloor facies related to upward methane flux within a Giant Pockmark of the
532 Lower Congo Basin. *Marine Geology*, **226**, 81–95.

533
534 GEE, M.J., MASSON, D.G., WATTS, A.B. & MITCHELL, N.C. (2001). - Passage of debris
535 flows and turbidity currents through a topographic constriction: seafloor erosion and
536 deflection of flow pathways. *Sedimentology*, **48**, 1389–1409.

537
538 GEE, M.J.R., MASSON, D.G., WATTS, A.B. & ALLEN, P.A. (1999). - The Saharan
539 debris\pounds ow: an insight into the mechanics of long runout submarine debris\pounds ows.
540 *Sedimentology*, **46**, 317–335.

541
542 GEORGIPOULOU, A., KRASTEL, S., MASSON, D.G. & WYNN, R.B. (2007). - Repeated
543 instability of the NW African margin related to buried landslide scarps. *In: Submarine Mass*
544 *Movements and Their Consequences*. Springer, 29–36.

545
546 GEORGIPOULOU, A., WYNN, R.B., MASSON, D.G. & FRENZ, M. (2009). - Linked
547 turbidite–debrite resulting from recent Sahara Slide headwall reactivation. *Marine and*
548 *Petroleum Geology*, **26**, 2021–2031.

549
550 GEORGIPOULOU, A., MASSON, D.G., WYNN, R.B. & KRASTEL, S. (2010). - Sahara
551 Slide: Age, initiation, and processes of a giant submarine slide. *Geochemistry, Geophysics,*
552 *Geosystems*, **11**.

553
554 HASIOTIS, T., PAPATHEODOROU, G., BOUCKOVALAS, G., CORBAU, C. & FERENTINOS, G.
555 (2002). - Earthquake-induced coastal sediment instabilities in the western Gulf of Corinth,
556 Greece. *Marine Geology*, **186**, 319–335.

557
558 HAYES, D.E. & RABINOWITZ, P.D. (1975). - Mesozoic magnetic lineations and the
559 magnetic quiet zone off northwest Africa. *Earth and Planetary Science Letters*, **28**, 105–115.

560
561 HENRICH, R., HANEUBUTH, T.J., KRASTEL, S., NEUBERT, N. & WYNN, R.B. (2008).
562 Architecture and sediment dynamics of the Mauritania Slide Complex. *Marine and Petroleum*
563 *Geology*, **25**, 17–33.

564
565 HOVLAND, M. (1984). - Gas-induced erosion features in the North Sea. *Earth Surface*
566 *Processes and Landforms*, **9**, 209–228.

567
568 HOVLAND, M. & JUDD, A.G. (1988). - *Seabed Pockmarks and Seepages: Impact on*
569 *Geology, Biology and the Marine Environment*.

570
571 HOVLAND, M. & SOMMERVILLE, J.H. (1985). - Characteristics of two natural gas
572 seepages in the North Sea. *Marine and Petroleum Geology*, **2**, 319–326.

573

574 HOVLAND, M., TALBOT, M.R., QVALE, H., OLAUSSEN, S. & AASBERG, L. (1987). -
575 Methane-related carbonate cements in pockmarks of the North Sea. *Journal of Sedimentary*
576 *Research*, **57**.

577 HOVLAND, M., GARDNER, J.V. & JUDD, A.G. (2002). - The significance of pockmarks
578 to understanding fluid flow processes and geohazards. *Geofluids*, **2**, 127–136.
579

580 HOVLAND, M., HEGGLAND, R., DE VRIES, M.H. & TJELTA, T.I. (2010). - Unit-
581 pockmarks and their potential significance for predicting fluid flow. *Marine and Petroleum*
582 *Geology*, **27**, 1190–1199.
583

584 HÜHNERBACH, V. & MASSON, D.G. (2004). - Landslides in the North Atlantic and its
585 adjacent seas: an analysis of their morphology, setting and behaviour. *Marine Geology*, **213**,
586 343–362.
587

588 JACOBI, R.D. (1976). - Sediment slides on the northwestern continental margin of
589 Africa. *Marine Geology*, **22**, 157–173.
590

591 JACOBI, R.D. & HAYES, D.E. (1992). - Northwest African continental rise: effects of
592 near-bottom processes inferred from high-resolution seismic data. *Geologic Evolution of*
593 *Atlantic Continental Rises, Van Nostrand Reinhold, New York*, 293–326.
594

595 JOLIVET, J.L., BONNIN, J., BEUZART, P. & AUZENDE, J.-M. (1984). - Cinématique de
596 l'Atlantique nord et central. *Publications du CNEXO Série Rapports scientifiques et*
597 *techniques*, **54**, 1–108.
598

599 JUDD, A. & HOVLAND, M. (2007). - Shallow gas and gas hydrates. *In: Seabed Fluid*
600 *Flow*. Cambridge University Press.
601

602 KARAKAŞ, G., NOWALD, N., BLAAS, M., MARCHESIELLO, P., FRICKENHAUS, S. &
603 SCHLITZER, R. (2006). - High-resolution modeling of sediment erosion and particle transport
604 across the northwest African shelf. *Journal of Geophysical Research: Oceans (1978–2012)*,
605 **111**.
606

607 KLINGELHOEFER, F., LABAILS, C., COSQUER, E., ROUZO, S., GÉLI, L., ASLANIAN, D.,
608 OLIVET, J.-L., SAHABI, M., NOUZÉ H. & UNTERNEHR, P. (2009). - Crustal structure of the SW-
609 Moroccan margin from wide-angle and reflection seismic data (the DAKHLA experiment)
610 Part A: Wide-angle seismic models. *Tectonophysics*, **468**, 63–82.
611

612 KRASTEL, S., WYNN, R.B., GEORGIPOULOU, A., GEERSEN, J., HENRICH, R., MEYER,
613 M. & SCHWENK, T. (2012). - Large-scale mass wasting on the Northwest African Continental
614 Margin: some general implications for mass wasting on passive continental margins. *In:*
615 *Submarine Mass Movements and Their Consequences*. Springer, 189–199.
616

617 KRASTEL, S., WYNN, R.B., HANEBUTH, T.J.J., HENRICH, R., HOLZ, C., MEGGERS, H.,
618 KUHLMANN, H., GEORGIPOULOU, A. & SCHULZ, H.D. (2006). - Mapping of seabed
619 morphology and shallow sediment structure of the Mauritania continental margin, Northwest
620 Africa: some implications for geohazard potential. *NORSK GEOLOGISK TIDSSKRIFT*, **86**,
621 163.
622

623 LABAILS, C. (2007). - La Marge Sud-Marocaine et Les Premières Phases D'ouverture
624 de L'océan Atlantique Central. Thèse de doctorat, Université de Bretagne Occidentale.
625
626
627 LABAILS, C., OLIVET, J.-L., ASLANIAN, D. & ROEST, W.R. (2010). - An alternative early
628 opening scenario for the Central Atlantic Ocean. *Earth and Planetary Science Letters*, **297**,
629 355–368.
630
631 LARRASOÑA, J.C., ROBERTS, A.P. & ROHLING, E.J. (2013). - Dynamics of Green
632 Sahara Periods and Their Role in Hominin Evolution. *PLoS ONE*, **8**, e76514, doi:
633 10.1371/journal.pone.0076514.
634
635 LEE, S.H. & CHOUGH, S.K. (2001). - High-resolution (2–7 kHz) acoustic and geometric
636 characters of submarine creep deposits in the South Korea Plateau, East Sea. *Sedimentology*,
637 **48**, 629–644.
638
639 LEE, S.H., CHOUGH, S.K., BACK, G.G., KIM, Y.B. & SUNG, B.S. (1999). - Gradual
640 downslope change in high-resolution acoustic characters and geometry of large-scale
641 submarine debris lobes in Ulleung Basin, East Sea (Sea of Japan), Korea. *Geo-Marine*
642 *Letters*, **19**, 254–261.
643
644 LONERGAN, L., JAMIN, N.H., JACKSON, C.A.-L. & JOHNSON, H.D. (2013). - U-shaped
645 slope gully systems and sediment waves on the passive margin of Gabon (West Africa).
646 *Marine Geology*, **337**, 80–97, doi: 10.1016/j.margeo.2013.02.001.
647
648 LONSDALE, P. (1982). - Sediment drifts of the Northeast Atlantic and their relationship
649 to the observed abyssal currents. *Bull. Inst. Geol. Bassin Aquitaine*, **31**, 141–149.
650
651 MASSON, D.G., VAN NIEL, B. & WEAVER, P.P.E. (1997). - Flow processes and
652 sediment deformation in the Canary debris flow on the NW African continental rise.
653 *Sedimentary Geology*, **110**, 163–179.
654
655 MASSON, D.G., WYNN, R.B. & TALLING, P.J. (2010). - Large landslides on passive
656 continental margins: processes, hypotheses and outstanding questions. *In: Submarine Mass*
657 *Movements and Their Consequences*. Springer, 153–165.
658
659 MCGEE, D., WINCKLER, G., STUUT, J.B.W. & BRADTMILLER, L.I. (2013). - The
660 magnitude, timing and abruptness of changes in North African dust deposition over the last
661 20,000 yr. *Earth and Planetary Science Letters*, **371**, 163–176.
662
663 MITTELSTAEDT, E. (1991). - The ocean boundary along the northwest African coast:
664 Circulation and oceanographic properties at the sea surface. *Progress in Oceanography*, **26**,
665 307–355, doi: 10.1016/0079-6611(91)90011-A.
666
667 MOUNTAIN, G.S. & TUCHOLKE, B.E. (1985). - Mesozoic and Cenozoic geology of the
668 U.S. Atlantic continental slope and rise. United States, Van Nostrand Reinhold Co. : New
669 York, NY, United States, 293–341.
670
671 MULDER, T. & ALEXANDER, J. (2001). - The physical character of subaqueous
672 sedimentary density flows and their deposits. *Sedimentology*, **48**, 269–299.

673 PATRIAT, M. & LABAILS, C. (2006). - Linking the Canary and Cape-Verde Hot-Spots,
674 Northwest Africa. *Marine Geophysical Researches*, **27**, 201–215, doi: 10.1007/s11001-006-
675 9000-7.

676
677 PILCHER, R. & ARGENT, J. (2007). - Mega-pockmarks and linear pockmark trains on the
678 West African continental margin. *Marine Geology*, **244**, 15–32.

679
680 RANKE, U., VON RAD, U. & WISSMANN, G. (1982). - Stratigraphy, facies and tectonic
681 development of the on-and offshore Aaiun-Tarfaya Basin—A review. *In: Geology of the*
682 *Northwest African Continental Margin*. Springer, 86–105.

683
684 RIBOULOT, V., CATTANEO, A., BERNÉ, S., SCHNEIDER, R.R., VOISSET, M., IMBERT, P. &
685 GRIMAUD, S. (2012). - Geometry and chronology of late Quaternary depositional sequences in
686 the Eastern Niger Submarine Delta. *Marine Geology*, **319**, 1–20.

687
688 RIBOULOT, V., CATTANEO, A., SULTAN, N., GARZIGLIA, S., KER, S., IMBERT, P. &
689 VOISSET, M. (2013). - Sea-level change and free gas occurrence influencing a submarine
690 landslide and pockmark formation and distribution in deepwater Nigeria. *Earth and Planetary*
691 *Science Letters*, **375**, 78–91.

692
693 RIBOULOT, V., THOMAS, Y., BERNÉ, S., JOUET, G. & CATTANEO, A. (2014). - Control of
694 Quaternary sea-level changes on gas seeps. *Geophysical Research Letters*, **41**, 4970–4977.

695
696 SAHABI, M., ASLANIAN, D. & OLIVET, J.-L. (2004). - Un nouveau point de départ pour
697 l’histoire de l’Atlantique central. *Comptes Rendus Geoscience*, **336**, 1041–1052.

698
699 SARNTHEIN, M., THIEDE, J., PFLAUMANN, U., ERLLENKEUSER, H., FÜTTERER, D.,
700 KOOPMANN, B., LANGE, H., SEIBOLD, E. (1982). - Atmospheric and oceanic circulation
701 patterns off Northwest Africa during the past 25 million years. *In: Geology of the Northwest*
702 *African Continental Margin*. Springer, 545–604.

703
704 SIDDALL, M., ROHLING, E.J., ALMOGI-LABIN, A., HEMLEBEN, C., MEISCHNER, D.,
705 SCHMELZER, I. & SMEED, D.A. (2003). - Sea-level fluctuations during the last glacial cycle.
706 *Nature*, **423**, 853–858.

707
708 SKONIECZNY, C., BORY, A., BOUT-ROUMAZEILLES, V., ABOUCHAMI, W., GALER, S.,
709 CROSTA, X., DIALLO, A. & NDIAYE, T. (2013). - A three-year time series of mineral dust
710 deposits on the West African margin: sedimentological and geochemical signatures and
711 implications for interpretation of marine paleo-dust records. *Earth and Planetary Science*
712 *Letters*, **364**, 145–156.

713
714 SMITH, W.H. & SANDWELL, D.T. (1997). - Global sea floor topography from satellite
715 altimetry and ship depth soundings. *Science*, **277**, 1956–1962.

716
717 SULTAN, N., BOHRMANN, G., RUFFINE, L., PAPE, T., RIBOULOT, V., COLLIAT, J.-L., DE
718 PRUNELÈ, A., DENNIELOU, B., GARZIGLIA, S., HIMMLER, T., MARSET, T., PETERS, C., RABIU,
719 A. & WEI, J. (2014). - Pockmark formation and evolution in deep water Nigeria: Rapid
720 hydrate growth versus slow hydrate dissolution. *Journal of Geophysical Research: Solid*
721 *Earth*, **119**, 2679–2694.

722

723 TWICHELL, D.C. & ROBERTS, D.G. (1982). - Morphology, distribution, and
724 development of submarine canyons on the United States Atlantic continental slope between
725 Hudson and Baltimore Canyons. *Geology*, **10**, 408–412.

726
727 VAN CAMP, L., NYKJAER, L., MITTELSTAEDT, E. & SCHLITTENHARDT, P. (1991). -
728 Upwelling and boundary circulation off Northwest Africa as depicted by infrared and visible
729 satellite observations. *Progress in Oceanography*, **26**, 357–402.

730
731 VIANA, A.R. & REBESCO, M. (2007). - Economic and palaeoceanographic significance
732 of contourite deposits. *Geological Society of London*.

733
734 VÖRÖSMARTY, C.J., FEKETE, B.M., MEYBECK, M. & LAMMERS, R.B. (2000). - Global
735 system of rivers: Its role in organizing continental land mass and defining land-to-ocean
736 linkages. *Global Biogeochemical Cycles*, **14**, 599–621, doi: 10.1029/1999GB900092.

737
738 WAELBROECK, C., LABEYRIE, L., MICHEL, E., DUPLESSY, J., McMANUS, J., LAMBECK, K.,
739 BALBON, E. & LABRACHERIE, M. (2002). - Sea-level and deep water temperature changes derived
740 from benthic foraminifera isotopic records. *Quaternary Science Reviews*, **21**, 295–305.

741
742 WEI, J., PAPE, T., SULTAN, N., COLLIAT, J.-L., HIMMLER, T., RUFFINE, L., DE PRUNELE,
743 A., DENNIELOU, B., GARZIGLIA, S., MARSSET, T., PETERS, C. A., RABIU, A. & BOHRMANN, G..
744 (2015). - Gas hydrate distributions in sediments of pockmarks from the Nigerian margin—
745 Results and interpretation from shallow drilling. *Marine and Petroleum Geology*, **59**, 359–
746 370.

747
748 WIEN, K., HOLZ, C., KÖLLING, M. & SCHULZ, H.D. (2006). - Age models for pelagites
749 and turbidites from the Cap Timiris Canyon off Mauritania. *Marine and Petroleum Geology*,
750 **23**, 337–352.

751
752 WYNN, R.B., MASSON, D.G., STOW, D.A. & WEAVER, P.P. (2000). - The Northwest
753 African slope apron: a modern analogue for deep-water systems with complex seafloor
754 topography. *Marine and Petroleum Geology*, **17**, 253–265.

755
756 WYNN, R.B., WEAVER, P.P., MASSON, D.G. & STOW, D.A. (2002). - Turbidite
757 depositional architecture across three interconnected deep-water basins on the north-west
758 African margin. *Sedimentology*, **49**, 669–695.

759
760 YANG, J. & DAVIES, R.J. (2013). - Gravity-driven faults: Migration pathways for
761 recycling gas after the dissociation of marine gas hydrates. *Marine Geology*, **336**, 1–9.

762
763 ZÜHLSDORFF, C., HANEBUTH, T.J.J. & HENRICH, R. (2008). - Persistent quasi-periodic
764 turbidite activity off Saharan Africa and its comparability to orbital and climate cyclicities.
765 *Geo-Marine Letters*, **28**, 87–95.

766
767
768

769 **FIGURE CAPTIONS:**

770 **Figure 1:** Bathymetry and global relief map from [Smith and Sandwell, 1997] (Mercator
771 projection, WGS84). of the NW Africa margin showing the study area (Dakhla zone) and the
772 main morphologic features, described in literature like slides and debris flows (with a color
773 code depending on authors), canyon and channel systems and the upwelling location of NW
774 Africa. A green line underlines the isobath 1500 m. Insert box shows the profiles (seismic and
775 bathymetry) position retrieved during the Dakhla cruise.

776

777 **Figure 2:** Bathymetric map of the offshore Dakhla from SIMRAD EM300 acquired during
778 the Dakhla cruise and Slope-gradient (in degrees) map calculated from the bathymetry data. A
779 synthetic bathymetric profiles shows the global morphology of the continental slope from
780 upperslope (- 80 m) downslope (- 3000m).

781

782 **Figure 3:** Morphobathymetric interpretation on shaded relief map showing the main
783 morphological features and echo-character mapping showing the distribution of the different
784 echo types (see Figure 6) in the study area. Dakhla canyon is shown (in yellow) , ridges areas,
785 the depressions shown (in dark blue) on the mid-slope, scarps S1 and S2 (in red) on the
786 lower slope and a meandering canyon is still visible on the south western part.

787

788 **Figure 4:** Detailed bathymetric map of the Dakhla shallot-shaped canyon. The Dakhla canyon
789 is divided into 3 parts: the "proximal part" upslope which groups several incisions, the
790 "median part" which shows the enlarged part of the structure and the "distal part" which
791 channelises turbidites issued from the median part. The bathymetric profile (ab) across the
792 proximal part shows the sharp incision. Bathymetric profiles (cd) and (ef) across the median

793 part show the large morphology of incision. Bathymetric profile (gh) across distal part shows
794 the main enlarged canyon downslope.

795

796 **Figure 5:** Focus on the mid-slope area with the wavy morphologies (ridges) and depressions.
797 (B) Shaded relief map showing the examples of the evolution of depression (pockmarks) from
798 a circular to an elongated giant shape. Synthetic bathymetric profiles (1, 2, 3 and 4) show the
799 different bathymetric sections on 1) the wavy morphologies (ridges) 2) the combining two
800 depressions (pockmarks) ; 3) a circular depression (isolated pockmark), 4) elongated
801 depressions (giant pockmarks).

802

803 **Figure 6:** List of the main chirp "echo types" described in the investigated area: distinct
804 echoes (I) with facies I-1 and I-2, hyperbolic echoes (II) and Hard echoes (III) with facies III-
805 1 and facies III-2. The description of the echo and the area where it occurs are detailed in the
806 main text.

807

808 **Figure 7:** Dakhla seismic profile (AB profile) and interpretation showing the global
809 morphology of the continental slope and the main sedimentary layers (main surfaces; top
810 Jurassic, Cretaceous surfaces and Eocene surface [Labails, 2007]). The seismic profile shows
811 significant seismic undulations of the sedimentary layers parallel to the seabed (location of
812 the seismic profile AB on figure 1).

813

814 **Figure 8:** Dakhla seismic profile (CD profile) and interpretation showing the global
815 morphology of the continental slope and the main surface sedimentary layers (main surfaces;
816 top Jurassic, Cretaceous surfaces and Eocene surface in [Labails, 2007]). seismic profile across
817 scarp S1, scarp S2 and depressions. Insert box shows (Chirp subbottom seismic) profiles

818 across the scarp S1, scarp S2 and depressions. The seismic profile shows significant bulge of
819 the basement (location of the seismic profile CD on figure 1).

820

821 **Figure 9** : The chirp profiles P02 and interpretation (location on figure 5A) shows the
822 seafloor depression and bright spots in this depression and overpressure ridges. The
823 unconformity surface truncates the subjacent reflectors and is recovered by parallel
824 reflectors.

825

826 **Figure 10**: Schematic illustration of the influence of pockmarks on seafloor stability and
827 relationship with sea-level [Sea-level curve from Waelbroeck *et al.*, 2002]. The model is
828 based on seismic profiles and bathymetry interpretation, A): formation and the alignment
829 pockmarks at 2600 mwd during stage MIS 8 then sliding (scarp 1) event during stage MIS 7.
830 B): formation and the alignment pockmarks, at 2200 mwd during stage MIS 6 then sliding
831 during stage MIS 5 (scarp 2); C) (MIS 2 to 0) : formation and the alignment pockmarks at
832 1500 mwd during stage MIS 2 and probable future sliding (S3).

833

834

835

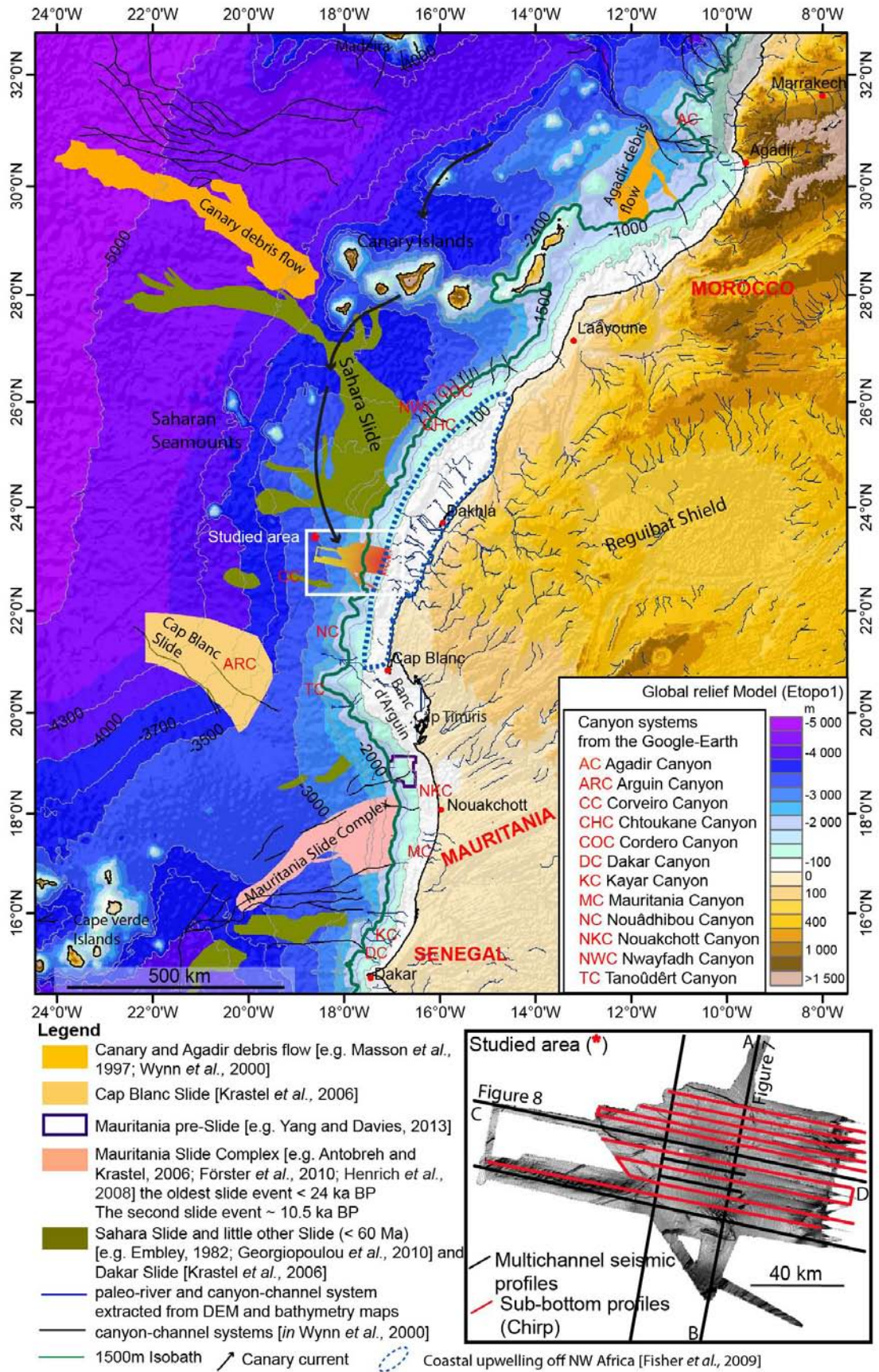
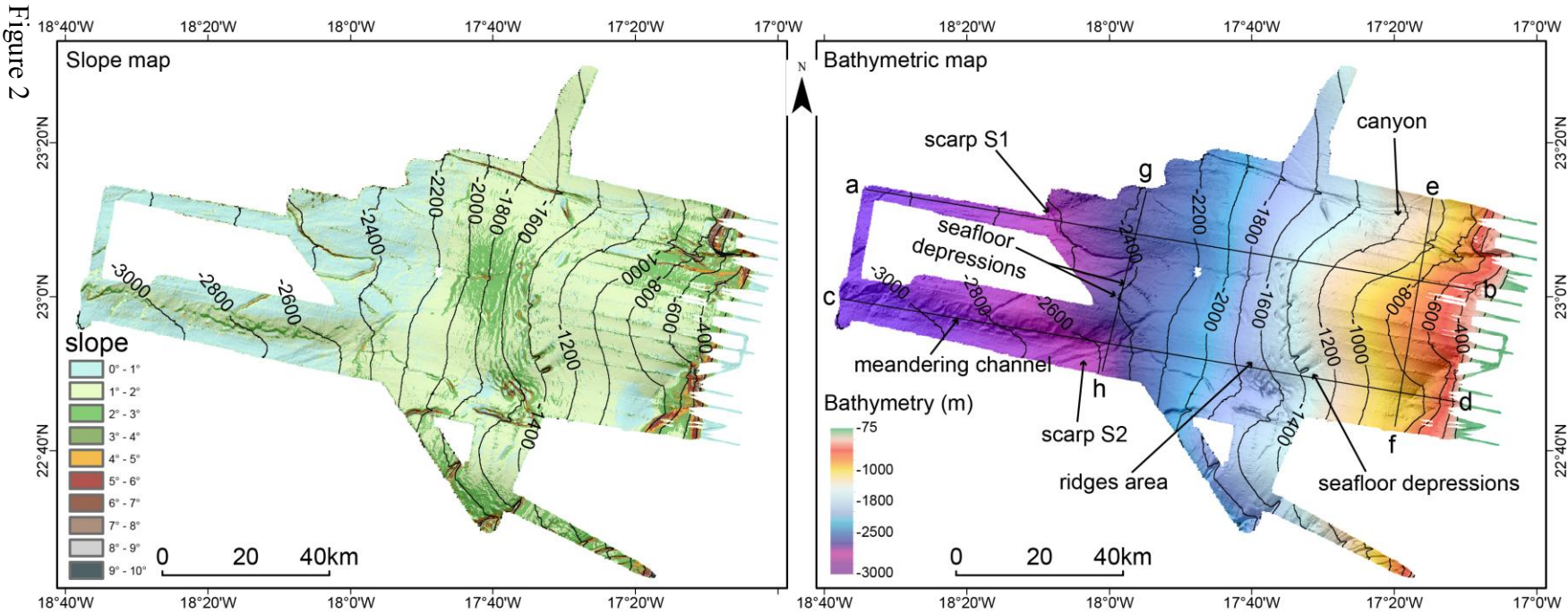


Figure 1

837
838
839



Bathymetric profiles

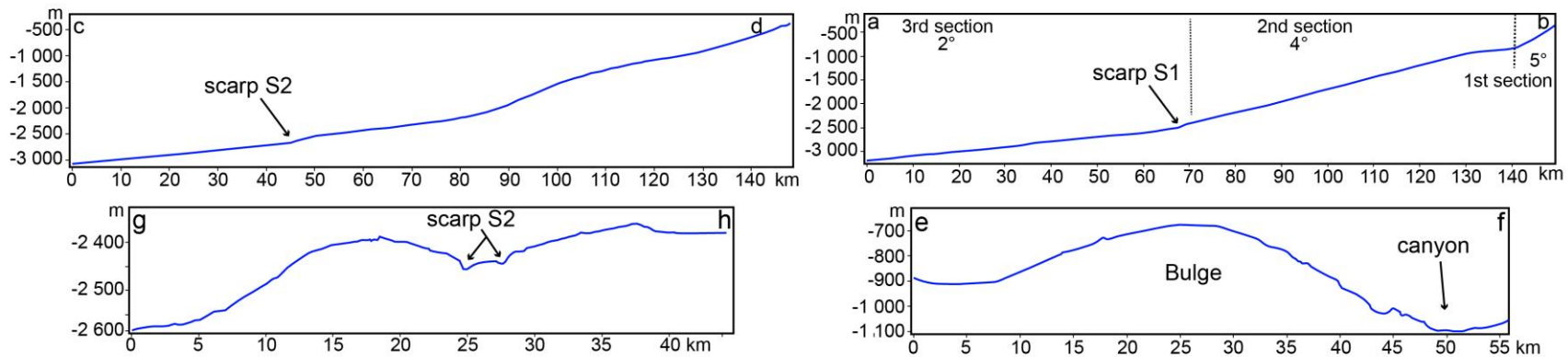
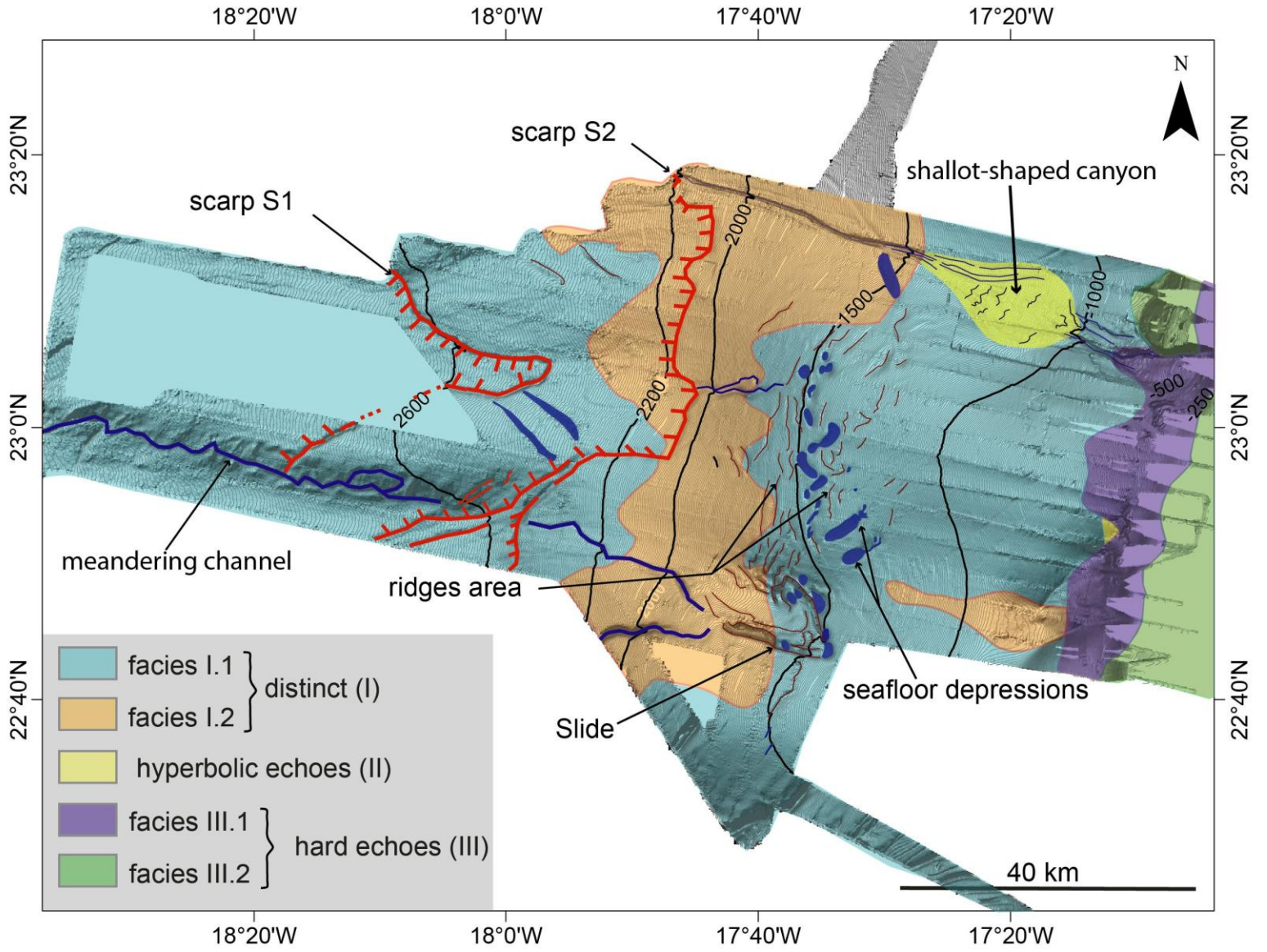
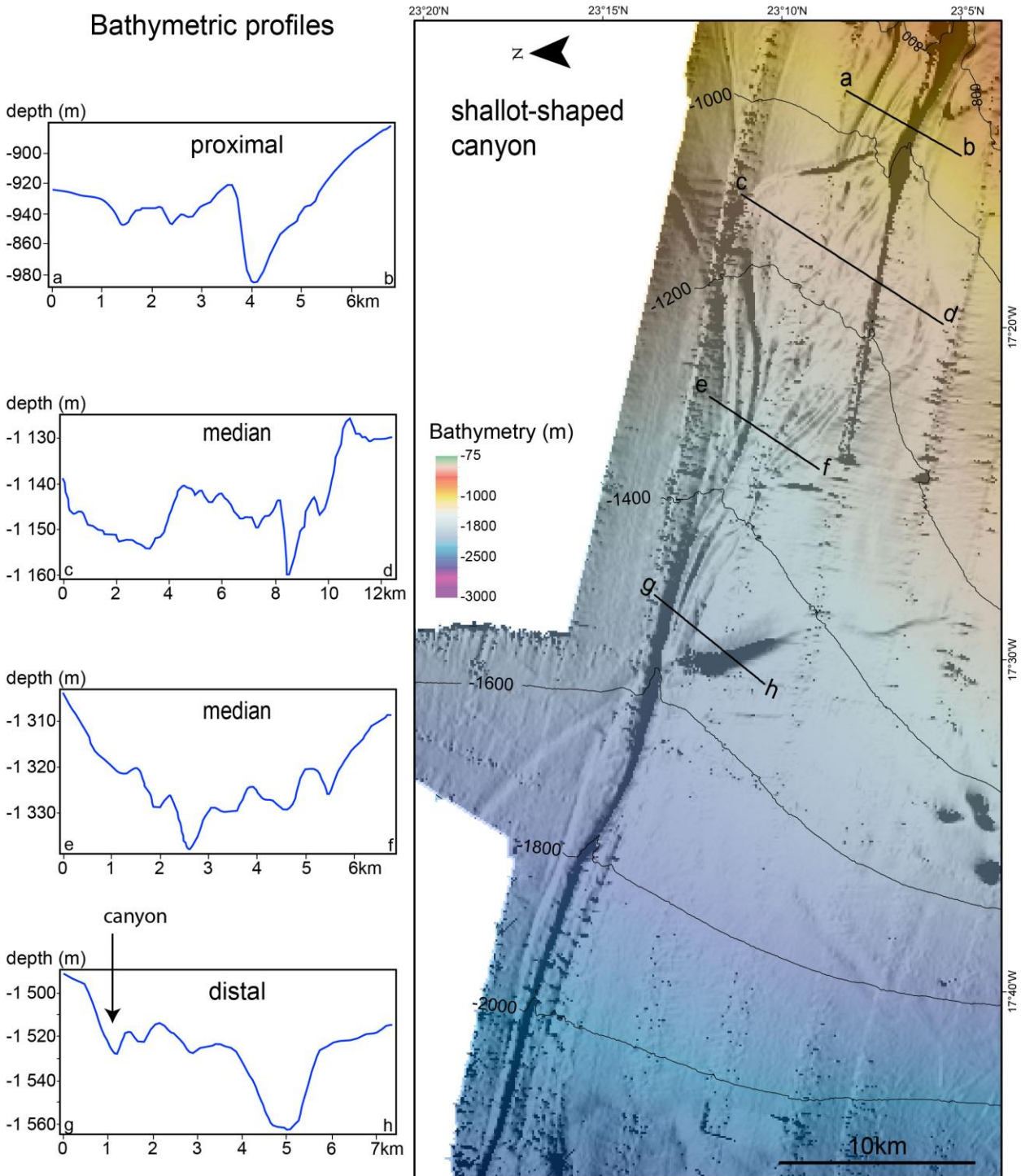


Figure 2

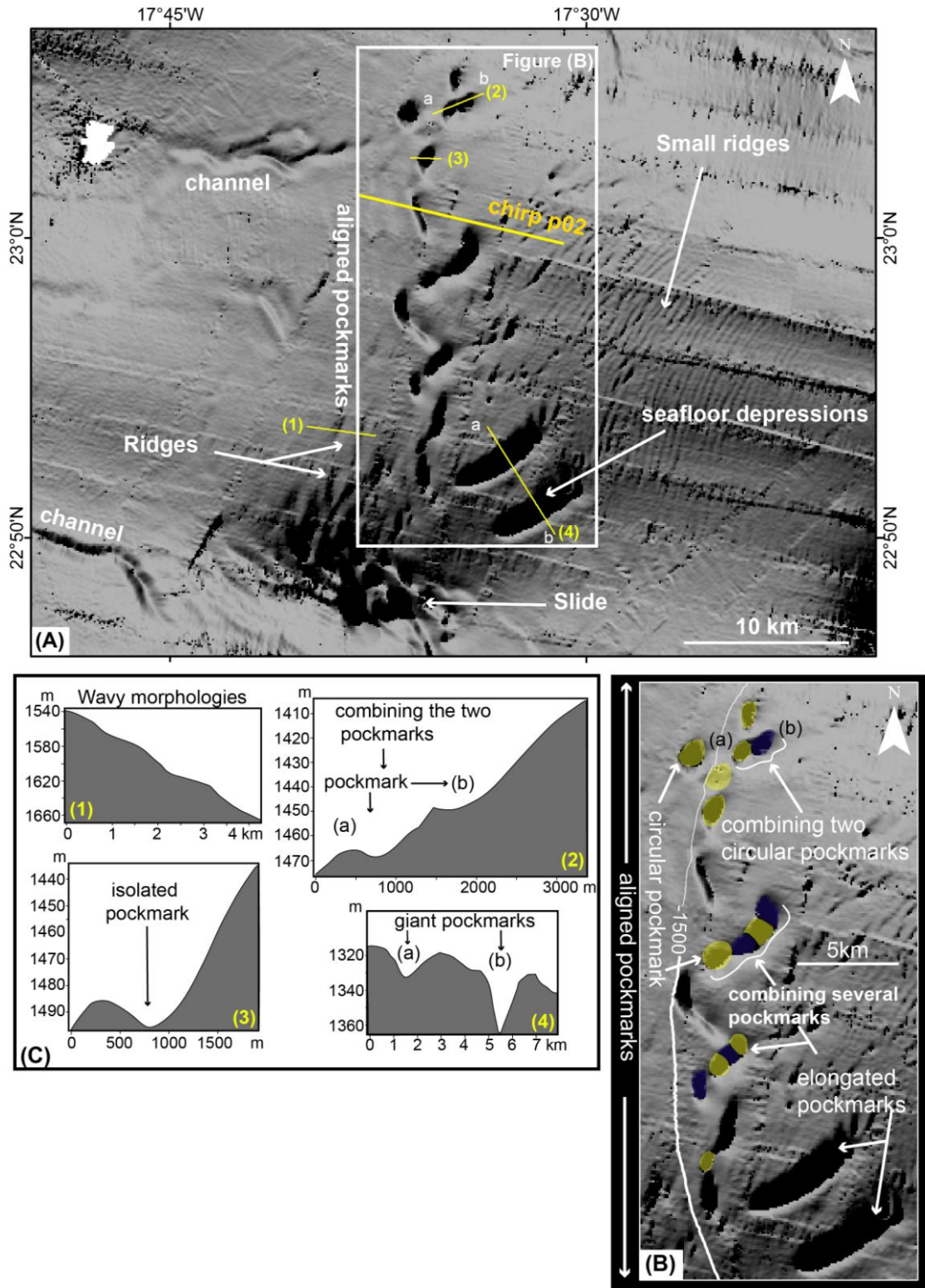
845
846
847
Figure 3




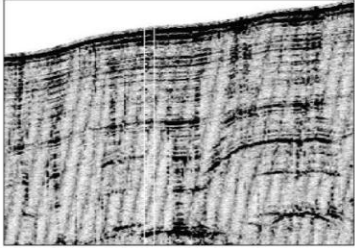

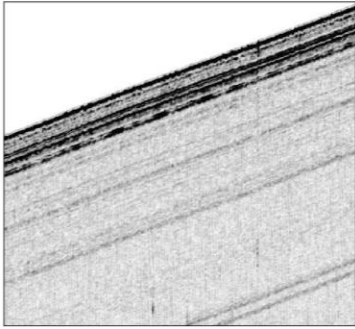
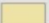
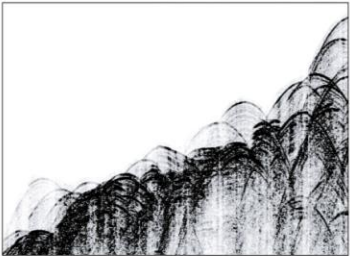

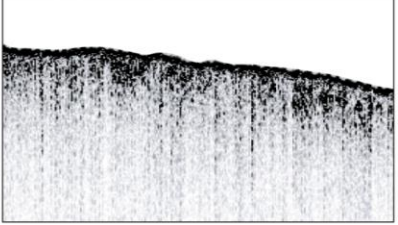
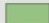
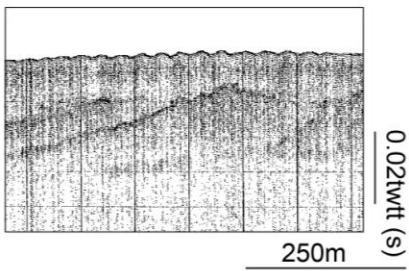


848
849
850
851
852

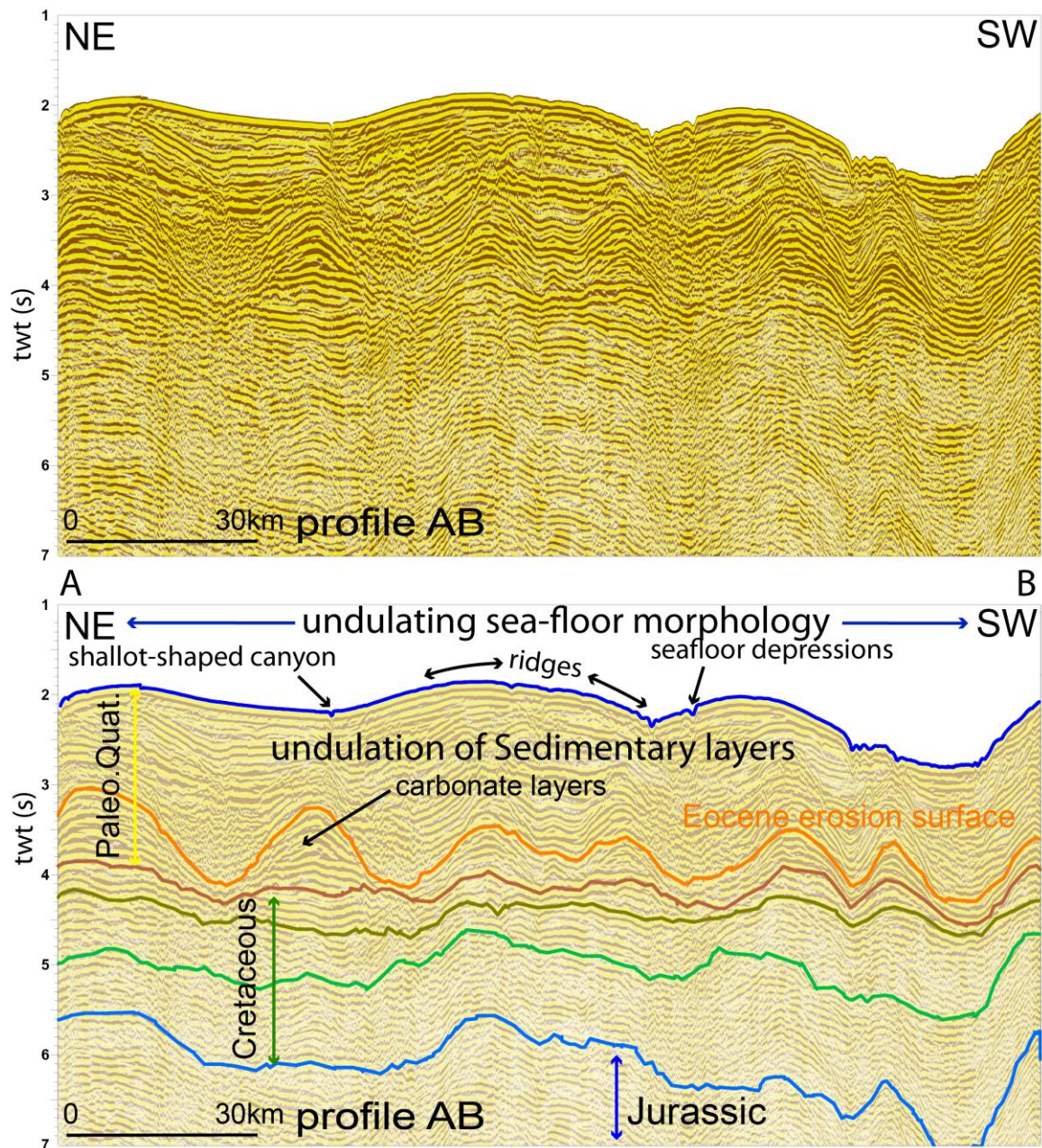
Figure 4



854
 855
 856 Figure 5
 857

Type		Type - Example	Zone	Description
distinct echoes (I)	facies I.1 		base continental slope and large part of the studied area	continuous and parallel reflectors of high amplitude and medium frequency
	facies I.2 		continental slope between 1600 and 2200	continuous and parallel reflectors with a transparent thin upper layer
hyperbolic echoes (II) 			mass transport deposits «troughs and holes»	is characterised by dense irregular overlapping hyperbolae
Hard echoes (III)	facies III.1 		upper continental slope	Hard facies is characterised by a dark surface reflector, with few or no sub-bottom reflectors
	facies III.2 		continental shelf	Hard subsurface with oblique reflectors (bed rock)

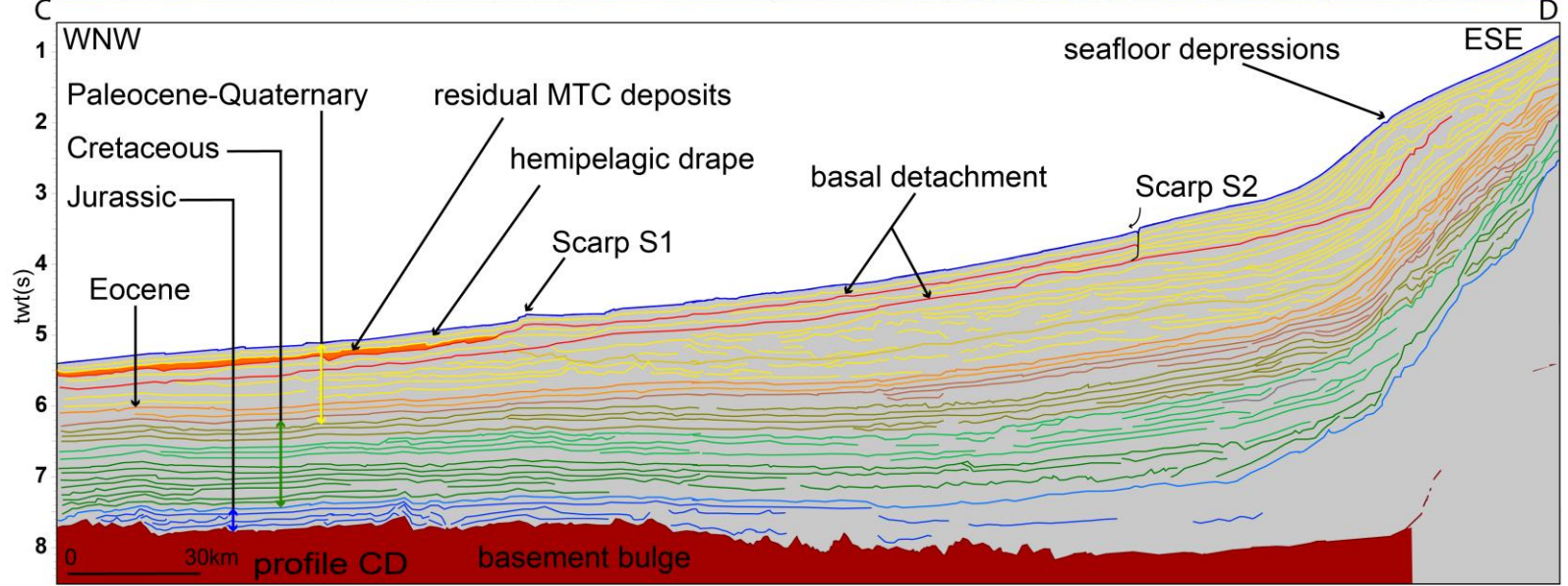
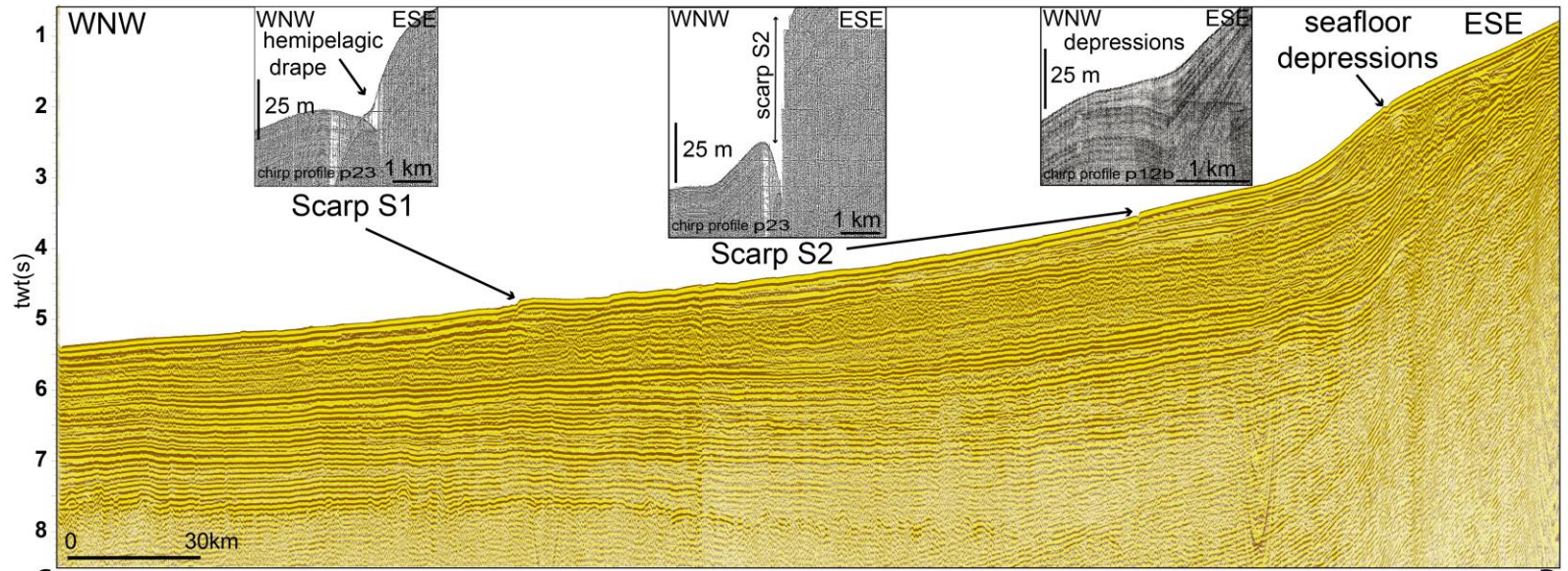
858
859 Figure 6
860

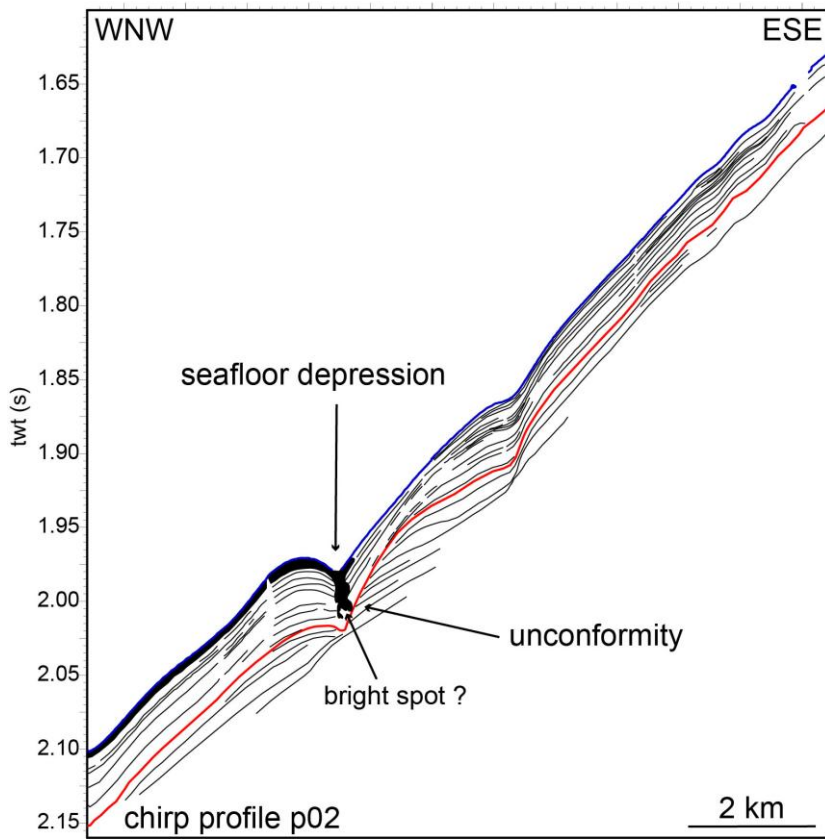
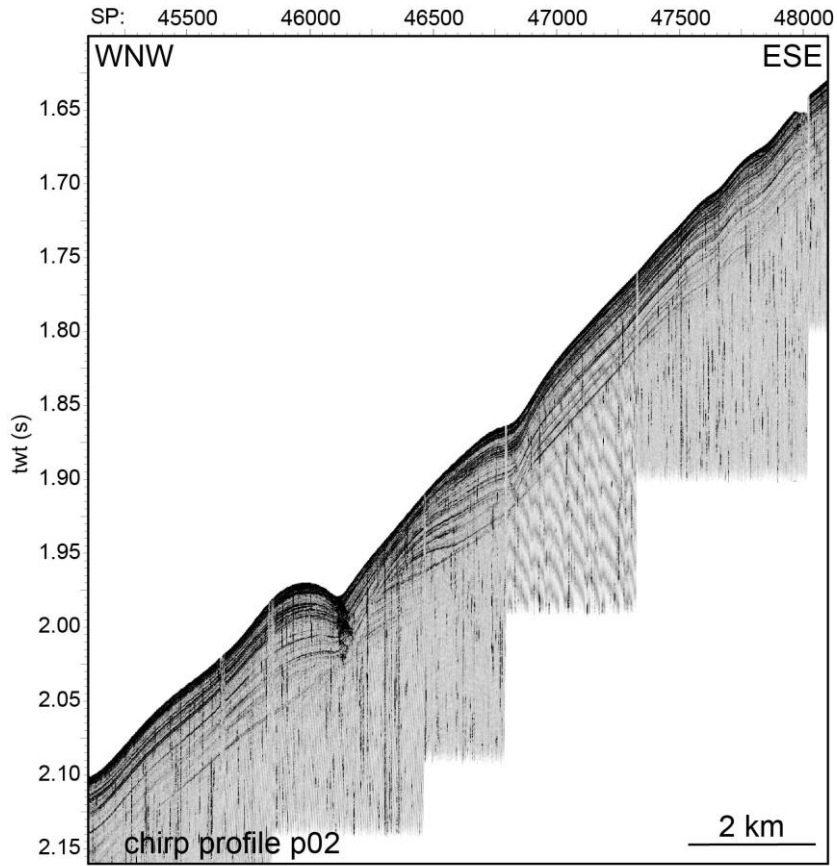


861
 862 Figure 7
 863

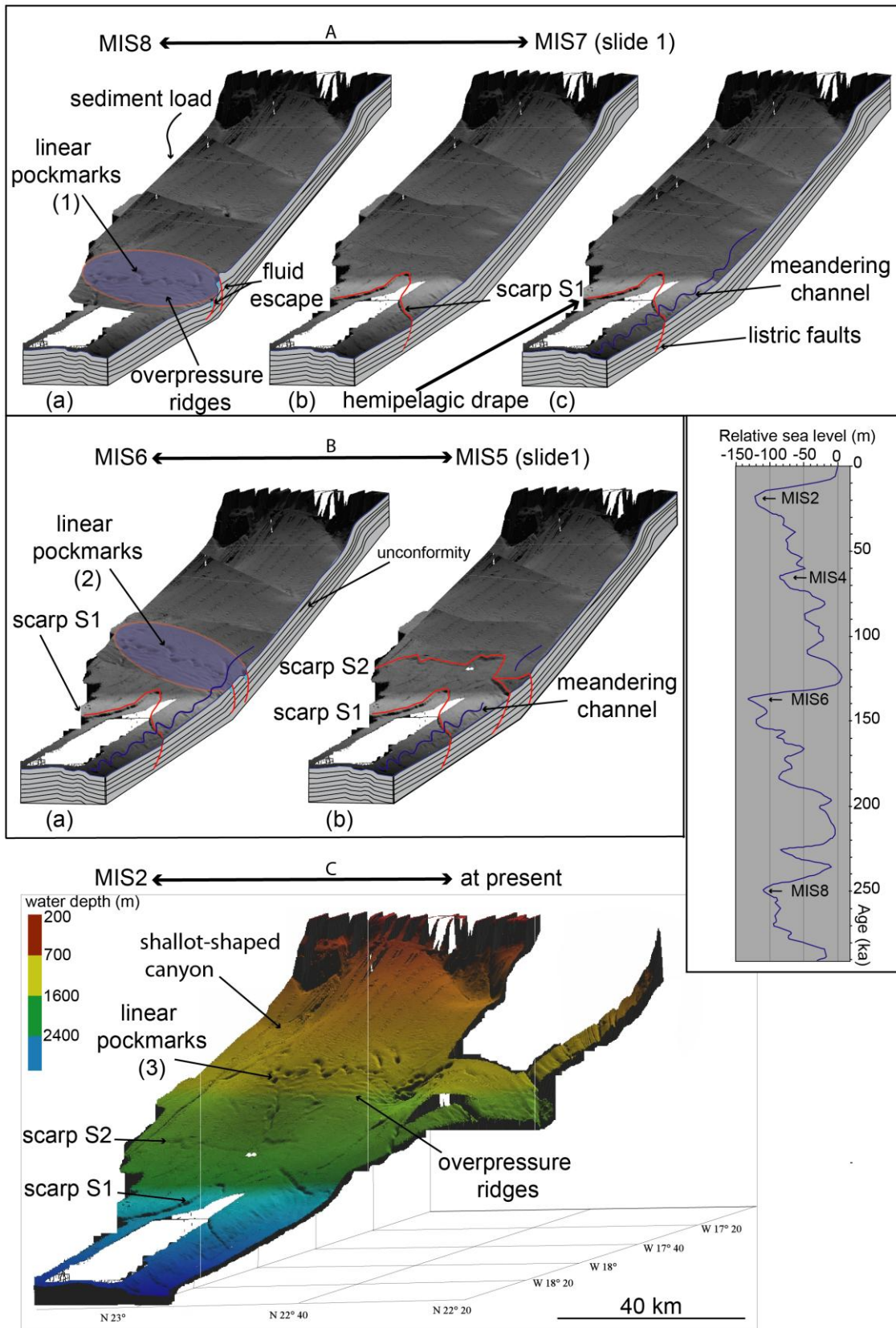
864
865
866
867

Figure 8





868
869 Figure 9
870



872
873 Figure 10
874